Publication Year	2015
Acceptance in OA@INAF	2020-07-07T11:59:05Z
Title	þÿ C a n t h e i n t e r g a l a c t i c m e d i u m c a u s e a r a p i d d r o p i n L y
Authors	Mesinger, Andrei; Aykutalp, Aycin; VANZELLA, Eros; PENTERICCI, Laura; Ferrara, Andrea; et al.
DOI	10.1093/mnras/stu2089
Handle	http://hdl.handle.net/20.500.12386/26363
Journal	MONTHLY NOTICES OF THE ROYAL ASTRONOMICAL SOCIETY
Number	446

Monthly Notices of the ROYAL ASTRONOMICAL SOCIETY

MNRAS **446,** 566–577 (2015) doi:10.1093/mnras/stu2089

Can the intergalactic medium cause a rapid drop in Lyα emission at $z > 6$?

Andrei Mesinger,[1]★ Aycin Aykutalp,[1] Eros Vanzella,[2] Laura Pentericci,[3] Andrea Ferrara[1] and Mark Dijkstra[4]

[1]*Scuola Normale Superiore, Piazza dei Cavalieri 7, I-56126 Pisa, Italy*
[2]*INAF Osservatorio Astronomico di Bologna, I-40127 Bologna, Italy*
[3]*INAF Osservatorio Astronomico di Roma, Via Frascatti 33, I-00040 Monteporzio, RM, Italy*
[4]*Institute of Theoretical Astrophysics, University of Oslo, Postboks 1029, 0858 Oslo, Norway*

Accepted 2014 October 6. Received 2014 October 6; in original form 2014 June 24

ABSTRACT

The large cross-section of the Lyα line makes it a sensitive probe of the ionization state of the intergalactic medium (IGM). Here, we present the most complete study to date of the IGM Lyα opacity, and its application to the redshift evolution of the 'Lyα fraction', i.e. the fraction of colour-selected galaxies with a detectable Lyα emission line. We use a tiered approach, which combines large-scale seminumeric simulations of reionization with moderate-scale hydrodynamic simulations of the ionized IGM. This allows us to simultaneously account for evolution in both: (i) the opacity from an incomplete (patchy) reionization, parametrized by the filling factor of ionized regions, $Q_{\rm H\,II}$; and (ii) the opacity from self-shielded systems in the ionized IGM, parametrized by the average photoionization rate inside H II regions, $\langle\Gamma_{12}\rangle_{\rm H\,II}$. In contrast to recent empirical models, attenuation from patchy reionization has a unimodal distribution along different sightlines, while attenuation from self-shielded systems is more bimodal. We quantify the average IGM transmission in our ($Q_{\rm H\,II}$, $\langle\Gamma_{12}\rangle_{\rm H\,II}$) parameter space, which can easily be used to interpret new data sets. Our new, improved models highly disfavour an evolution in $\langle\Gamma_{12}\rangle_{\rm H\,II}$ as the sole driver of a large change in IGM opacity. Using current observations, we predict that the Lyα fraction cannot drop by more than a factor of $\approx$2 with IGM attenuation alone, even for H II filling factors as low as $Q_{\rm H\,II} \gtrsim 0.1$. Larger changes in the Lyα fraction could result from a co-evolution with galaxy properties. Marginalizing over $\langle\Gamma_{12}\rangle_{\rm H\,II}$, we find that current observations constrain $Q_{\rm H\,II}(z \approx 7) \leq 0.6$, at a 68 per cent confidence level (CL). However, all of our parameter space is consistent with observations at 95 per cent CL, highlighting the need for larger observational samples at $z \geq 6$.

Key words: galaxies: evolution – intergalactic medium – cosmology: theory – dark ages, reionization, first stars – diffuse radiation – early Universe.

1 INTRODUCTION

The Lyα line from galaxies provides a window on the last frontier in astrophysical cosmology: the Epoch of Reionization (EoR). Lyα is strongly attenuated by neutral hydrogen, even in the damping wing of the line cross-section. Neutral patches of the intergalactic medium (IGM) could therefore significantly suppress the intrinsic Lyα line of galaxies during reionization (e.g. Miralda-Escude 1998; Haiman & Spaans 1999; Santos et al. 2004).

Extracting the imprint of reionization from galaxy observations at a single redshift is difficult, since we do not know how to a priori model the intrinsic Lyα line shape and luminosity, before it is processed by IGM absorption (see Section 2.4). Therefore, reionization constraints generally rely on the redshift *evolution* of Lyα observables, which allows one to assume that galaxy and line properties do not evolve over the same interval. Indeed, recently it was claimed that the fraction of colour-selected galaxies with a strong Lyα line [generally defined as having a rest-frame equivalent width (REW) greater than 25 Å], the so-called Lyα fraction, drops sharply from $z \approx 6 \rightarrow 7$; although interpretation is still limited by small number statistics (e.g. Stark et al. 2010; Pentericci et al. 2011; Ono et al. 2012; Caruana et al. 2014; Schenker et al. 2014). Absorption by neutral patches remaining from an incomplete reionization is often evoked as an obvious cause of such a drop.

However, the late stages of reionization are characterized by large cosmic H II regions. The remaining neutral patches are generally distant from galaxies, with a correspondingly weak damping wing

★ E-mail: andrei.mesinger@sns.it

© 2014 The Authors
Published by Oxford University Press on behalf of the Royal Astronomical Society

Downloaded from https://academic.oup.com/mnras/article-abstract/446/1/566/1322451 by guest on 03 June 2020

imprint on the Lyα line. A strong evolution in the Lyα fraction would therefore require a very substantial change in the filling factor of ionized regions, $Q_{\rm H\,II}$, over the same brief interval: $z \approx 6 \rightarrow 7$ (e.g. McQuinn et al. 2007; Mesinger & Furlanetto 2008b; Dijkstra, Mesinger & Wyithe 2011; Jensen et al. 2013). Alternately, if the photoionizing background drops rapidly beyond $z \gtrsim 6$, the increasing abundance of self-shielded systems inside the ionized IGM can imprint a similar signature (Bolton & Haehnelt 2013). Yet another possibility to explain a drop in the Lyα fraction is an evolution of the intrinsic galaxy properties themselves, such as wind characteristics and the escape fraction of ionizing photons, $f_{\rm esc}$ (Dijkstra et al. 2014). Alternately, a joint evolution in the IGM and/or galaxy properties could ease tension with observations.

Here, we develop the most comprehensive model of IGM absorption to date, including the impact of both (i) the large-scale (hundreds of cMpc; e.g. Iliev et al. 2014) reionization morphology; and (ii) ∼kpc scale (e.g. Schaye 2001) self-shielded systems. We make use of well-tested seminumerical simulations to model reionization morphology. Our reionization simulations include sub-grid modelling of UV photoheating feedback and recombinations, shown to significantly decrease the size of cosmic H II regions (Sobacchi & Mesinger 2014). We complement these with moderate-scale (tens of cMpc) hydrodynamic simulations of the ionized IGM, resolving the relevant self-shielded systems. With this tiered approach, we show how the redshift evolution in the $z \gtrsim 6$ Lyα fraction can constrain both the filling factor of ionized regions as well as the photoionizing background.

This paper is organized as follows. In Section 2, we present our model for IGM absorption, sourced by both patchy reionization (Section 2.1) and self-shielded systems (Section 2.2). In Section 3, we present our results on the evolution of the IGM transmission and the Lyα fraction from $z \approx 6 \rightarrow 7$. Finally, we conclude in Section 4.

Unless stated otherwise, we quote all quantities in comoving units. We adopt the background cosmological parameters: (Ω_Λ, $\Omega_{\rm M}$, $\Omega_{\rm b}$, n, σ_8, H_0) = (0.68, 0.32, 0.049, 0.96, 0.83, 67 km s^{-1} Mpc^{-1}), consistent with recent results from the *Planck* mission (Planck Collaboration XVI 2013).

2 MODEL

Because of the difficulties mentioned above, we model the total Lyα opacity using a tiered approach, illustrated in Fig. 1. We simulate the morphology of reionization on large scales (hundreds of Mpc), using a seminumeric simulation. The reionization simulation is used to compute the damping wing opacities from the large-scale distribution of cosmic neutral patches, for a given value of the H II volume filling factor, $Q_{\rm H\,II}$. We complement the reionization simulation with a moderate-scale (tens of Mpc) hydrodynamic simulation, capable of resolving self-shielding gas clumps in the cosmic ionized patches of the IGM surrounding high-z galaxies. The hydrodynamic

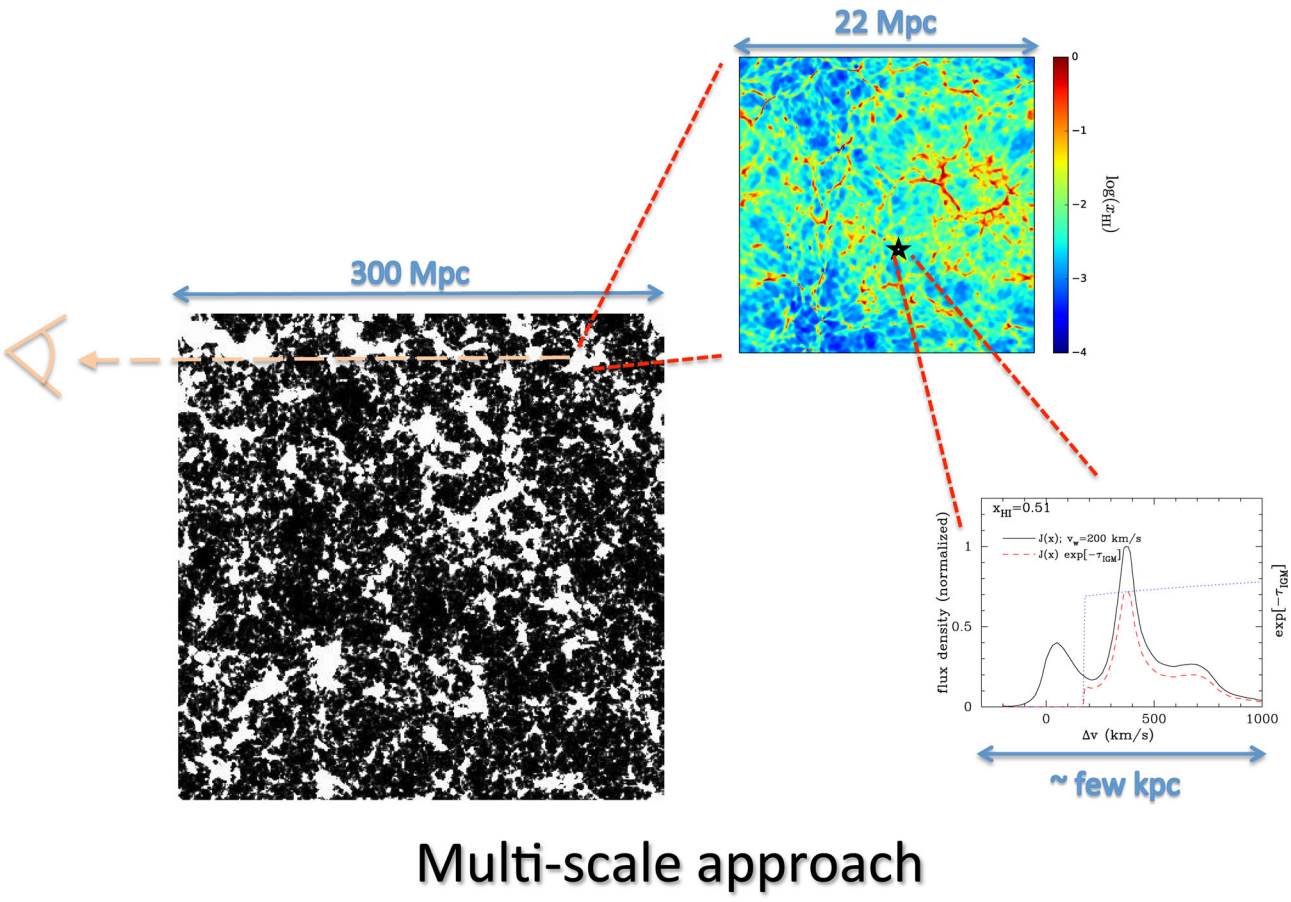

Figure 1. Schematic showing the various components of our model. From left to right we show: (i) a 0.75 Mpc thick slice through our large-scale reionization simulation at $Q_{\rm H\,II} \sim 0.5$, with cosmic H II (H I) patches shown in white (black) (Sobacchi & Mesinger 2014); (ii) a 21 kpc slice through our hydro simulation of the residual H I inside the cosmic H II patches surrounding high-z galaxies; (iii) the Lyα line emerging from a galaxy including RT through local outflows. (i) and (ii) are used in this work, while (iii) is taken from Dijkstra et al. (2011). Relative scales are approximate.

Downloaded from https://academic.oup.com/mnras/article-abstract/446/1/566/1322451 by guest on 03 June 2020

simulation is used to compute the opacities from high-column density systems, parametrized by the average photoionization rate inside the ionized patches of the IGM, $\langle\Gamma_{12}\rangle_{\rm H\,II}$. $Q_{\rm H\,II}$ and $\langle\Gamma_{12}\rangle_{\rm H\,II}$ are the two fundamental free parameters in our model of the IGM opacity. Note that $\langle\Gamma_{12}\rangle_{\rm H\,II}$ depends on the *instantaneous* ionizing emissivity and mean free path, while $Q_{\rm H\,II}$ depends (roughly) on the *time-integrated history* of these quantities. In principle, complete models of reionization could predict both $Q_{\rm H\,II}$ and $\langle\Gamma_{12}\rangle_{\rm H\,II}$ self-consistently (see the discussion in Section 3.4.2). However, as the relation between $Q_{\rm H\,II}$ and $\langle\Gamma_{12}\rangle_{\rm H\,II}$ is highly model-dependent and very uncertain, we leave these two quantities as free parameters.

Finally, to illustrate the effects of the Lyα line profile emerging from the galaxy, we assume a simple Gaussian profile, centred at various velocity offsets. Modelling the intrinsic Lyα emission is beyond the scope of this work. However, our models illustrate the relevant trends, showing that the derived constraints are not very sensitive to the profile (though they could be sensitive to a redshift *evolution* in the profile). Below we discuss the details of our model in turn.

2.1 Reionization morphology

We model the EoR morphology (i.e. large-scale pattern of ionized and neutral IGM patches) using the publicly available, seminumerical codes DEXM and 21CMFAST[1] (Mesinger & Furlanetto 2007; Mesinger, Furlanetto & Cen 2011). The seminumerical approach combines excursion set and perturbation formalisms to generate various cosmic fields, and has been extensively tested against numerical simulations (Mesinger & Furlanetto 2007; Mesinger et al. 2011; Zahn et al. 2011).

Our simulation box is 300 Mpc on a side with a resolution of 400^3. Our reionization fields are characterized by $Q_{\rm H\,II}$: the filling factor of H II regions, and are taken from Sobacchi & Mesinger (2014). The reionization simulations of Sobacchi & Mesinger (2014) include inhomogeneous, sub-grid modelling of (i) UV feedback on galaxies; and (ii) recombinations. Effect (i) results from the UV background (UVB) heating the accreting gas, thereby suppressing the star formation rate in low-mass galaxies inside cosmic H II regions (e.g. Efstathiou 1992; Shapiro, Giroux & Babul 1994; Hui & Gnedin 1997). Using suites of spherically symmetric cosmological hydro simulations, Sobacchi & Mesinger (2013) provided a parametrized fit for the resulting depletion of gas and effective critical halo mass capable of hosting star-forming galaxies. Likewise, (ii) accounts for inhomogeneous recombinations. These are driven by systems too small to be resolved in large-scale reionization simulations, and can be an important (and inhomogeneous) drain on the ionizing photon budget. Both (i) and (ii) depend on the thermal and ionization history of the local gas patch, on scales which are too small to be tracked in reionization simulations, without a sub-grid prescription. Furthermore, both effects are additive, in that they both preferentially impede the growth of large H II regions.

With the excursion set and perturbation theory approach outlined in Mesinger & Furlanetto (2007), we compute halo catalogues at $z = 7$ corresponding to the same initial conditions used to generate the EoR maps (sampled on a higher resolution 1600^3 grid). We generate 5000 randomly oriented sightlines, originating from 100 haloes with masses $M_{\rm halo} \approx 10^{10.5-11}\,{\rm M}_\odot$, roughly corresponding to the host halo masses of the observed population of high-z galaxies, inferred through abundance matching and clustering (e.g. Ouchi et al. 2010).

For each sightline originating from a DM halo, we sum the optical depth contribution of neutral patches along the line of sight (LOS), out to a distance of $R_{\rm max} = 100$Mpc:

$$\tau_{\rm reion}(Q_{\rm H\,II}) = \int_{R_{\rm H\,II}}^{R_{\rm max}} d\tau_{\rm reion}, \quad (1)$$

where $R_{\rm H\,II}$ is the distance from the host halo to the first cosmic neutral patch along the randomly-oriented sightline (what we refer to below as the size of the local cosmic H II region). Each neutral patch (extending from $z_{\rm begin}$ to $z_{\rm end}$) encountered along the LOS contributes to the damping wing optical depth according to (e.g. Miralda-Escude 1998):

$$d\tau_{\rm reion} = 6.43\times10^{-9}\left(\frac{\pi e^2 f_\alpha n_{\rm H}(z)}{m_{\rm e}cH(z_{\rm s})}\right) \times\left[I\left(\frac{1+z_{\rm begin}}{8}\right) - I\left(\frac{1+z_{\rm end}}{8}\right)\right], \quad (2)$$

where $\bar{n}_{\rm H}$ is the mean hydrogen number density and

$$I(x) \equiv \frac{x^{9/2}}{1-x} + \frac{9}{7}x^{7/2} + \frac{9}{5}x^{5/2} + 3x^{3/2} + 9x^{1/2} - \ln\left|\frac{1+x^{1/2}}{1-x^{1/2}}\right|.$$

The resulting distributions of reionization opacities, $\exp[-\tau_{\rm reion}]$, are shown in Fig. 2, as functions of the velocity offset from the systemic redshift of the galaxy (shown as a vertical dashed line). Panels correspond to $Q_{\rm H\,II} = 0.20, 0.50, 0.77$, (*left to right*).

During the advanced stages of reionization, most galaxies reside in large H II regions, suffering from only modest absorption from the remaining neutral patches. This is further illustration that the observability of galactic Lyα emission does not evolve dramatically during the end stages of reionization (e.g. Furlanetto, Zaldarriaga & Hernquist 2006).

Furthermore, the sightline-to-sightline scatter in the optical depth, $\tau_{\rm reion}$, rapidly increases as reionization progresses: some sightlines go through long stretches of the ionized IGM, while others encounter neutral material close to the galaxies. Indeed, given enough sightlines, this scatter itself can be used as a probe of reionization (Mesinger & Furlanetto 2008a). Although the sightline-to-sightline scatter is large, individual sightlines have damping wing opacities which are smooth functions of wavelength (e.g. Miralda-Escude 1998). One example sightline is illustrated with a green curve in the panels of Fig. 2.

2.1.1 *The role of IGM recombinations and UVB feedback in shaping reionization morphology*

Using a sub-grid model of inhomogeneous recombinations, Sobacchi & Mesinger (2014) recently showed that UVB photoheating and, more importantly, recombinations in the IGM (driven by systems too small to be resolved in large-scale reionization simulations) can dramatically suppress large-scale ionization structure. Previous studies of the Lyα opacity from a patchy EoR did not include sub-grid recombinations (e.g. McQuinn et al. 2007; Iliev et al. 2008; Mesinger & Furlanetto 2008b; Dijkstra et al. 2011; Jensen et al. 2013; Taylor & Lidz 2014), and only included UVB feedback on sources via an ad hoc, 'on-off' treatment (e.g. Iliev et al. 2008; Jensen et al. 2013). Here, we highlight how these new, physically

[1] http://homepage.sns.it/mesinger/Sim

Downloaded from https://academic.oup.com/mnras/article-abstract/446/1/566/1322451 by guest on 03 June 2020

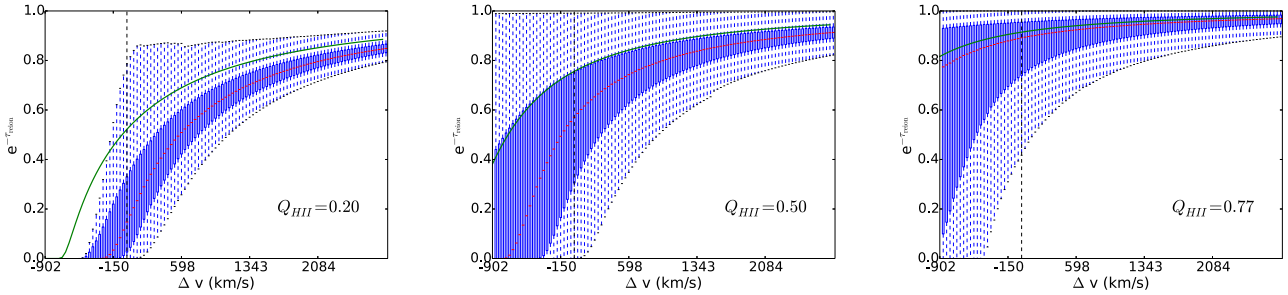

Figure 2. Distributions of the damping wing transmission from an inhomogeneous reionization, as functions of the rest-frame velocity offset from the Lyα line centre (shown as a vertical dashed line). Panels correspond to $Q_{\rm H\,II} = 0.20, 0.50, 0.77$, (left to right). Red lines correspond to the median profile, while boxes/whiskers enclose the first two quartiles of the distribution. The scatter represents the sightline-to-sightline scatter, but it should be noted that damping wings of individual sightlines are smooth functions of wavelength. Absorption profiles from a sample sightline are overplotted with green curves.

motivated reionization models change prior interpretation of the Lyα opacity during the EoR.

In agreement with analytic estimates (Furlanetto & Oh 2005), at $Q_{\rm H\,II} \gtrsim 0.9$ reionization progresses in a recombination-limited fashion, with recombinations balancing ionizations in large H II regions. However, recombinations slow the growth of H II regions well before this cosmic Strömgren limit, resulting in a more uniform reionization morphology with a dramatic suppression of large H II regions. Typical H II regions sizes are smaller by factors of ∼2–3 throughout reionization (fig. 7 in Sobacchi & Mesinger 2014). This 'feedback-limited'morphology is important because smaller H II regions increase the imprint of neutral cosmic gas on the Lyα emission line. Hence the change in $Q_{\rm H\,II}$ required to explain a given drop in the Lyα fraction would be reduced, when compared to prior studies.

We show the impact of these feedback-limited reionization morphologies on the Lyα transmission in Fig. 3. These cumulative distribution functions are constructed from our 5000 sightlines, and evaluated at a single wavelength, $\Delta v = 200\,{\rm km\,s^{-1}}$ redwards of the systemic galaxy redshift. Solid curves correspond to our fiducial reionization morphologies, while the dot–dashed curves correspond to previous estimates which ignore the role of inhomogeneous recombinations and UV feedback in suppressing large H II regions. From the figure, we see that our opacity distribution at $Q_{\rm H\,II} = 0.7$ is similar to the one at an earlier stage in reionization, $Q \approx 0.5$–0.6, using morphologies not taking into account recombinations and UVB feedback. Hence, we already expect that the Lyα fraction constraints on $Q_{\rm H\,II}(z = 7)$ will relax by $\Delta Q_{\rm H\,II} \sim 0.1 - 0.2$, when taking into account new, feedback-limited morphologies.

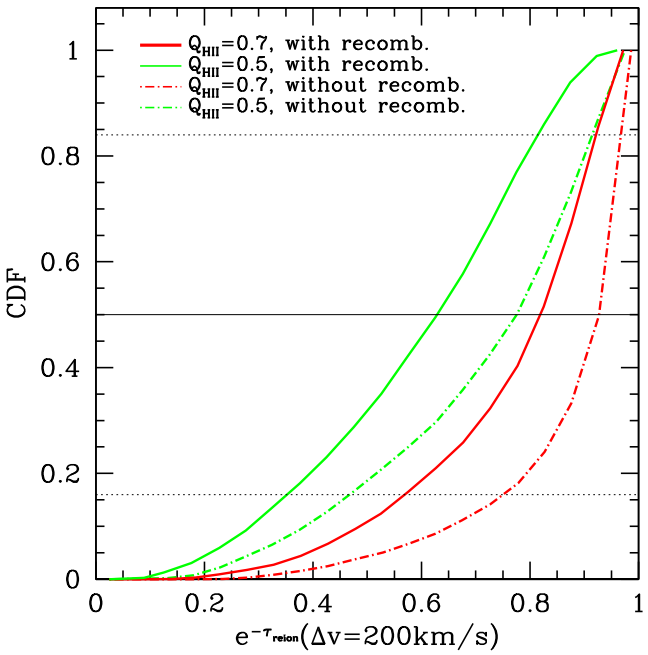

Figure 3. Fraction of sightlines having reionization transmission less than $\exp[-\tau_{\rm reion}]$, evaluated at $\Delta v = 200\,{\rm km\,s^{-1}}$ redwards of the galaxy's systemic redshift. The median and 68 per cent contours are shown with thin horizontal lines. Curves correspond to $Q_{\rm H\,II} = 0.5, 0.7$ (left to right). The importance of self-consistently including IGM recombinations (and UVB feedback) is shown by comparing the solid to the dot–dashed curves. The former corresponds to our fiducial reionization morphology (taken from Sobacchi & Mesinger 2014), while the later corresponds to the common approach of a redshift-independent minimum mass for star-forming galaxies (here taken to be $M_{\rm halo} = 5 \times 10^8\,{\rm M}_\odot$), and more importantly, ignoring the impact of inhomogeneous recombinations in the IGM.

2.2 Inside the ionized patches of the IGM

Even before reionization completes, each galaxy is embedded inside a cosmic H II patch. In the advanced stages of reionization, these H II patches (or bubbles) are sourced by the large-scale distribution of star formation histories of thousands of galaxies (e.g. Furlanetto, Zaldarriaga & Hernquist 2004). The residual volume-weighted neutral fraction inside the ionized IGM is fairly modest (e.g. $\langle x_{\rm H\,I}\rangle_{\rm H\,II} \sim 10^{-3}$–$10^{-4}$ at $z \sim 6$; e.g. Fan et al. 2006) However, self-shielded systems [damped Lyα systems (DLAs) and sub-DLAs] inside the ionized IGM could retain enough neutral hydrogen to imprint strong damping wing absorption. If the local ionizing radiation is weak, sightlines through the ionized IGM could have a relatively high incidence of self-shielded systems. Bolton & Haehnelt (2013) recently suggested this can have a large impact on the $z \approx 7$ Lyα fraction.

We model the ionized IGM surrounding Lyα emitting galaxies with the cosmological hydrodynamic code ENZO[2] v2.2 (The Enzo Collaboration 2014). Our simulation boxes are 22 Mpc on a side. The root grid is 256^3, and we have four additional levels of hydro-refinement resulting in a final baryon resolution of 0.66 proper kpc

[2] http://enzo-project.org/

Downloaded from https://academic.oup.com/mnras/article-abstract/446/1/566/1322451 by guest on 03 June 2020

(pkpc) at $z = 7$, which resolves the Jeans length of the relevant systems by a factor of $\sim$10. Note that the Jeans length can be written as $L_{\rm J} = 7.4\ {\rm pkpc}(\frac{T}{10^4\ {\rm K}})^{0.44}(\frac{\Gamma_{12}}{0.1})^{-1/3}(\frac{\Delta}{10\Delta_{\rm ss}})^{-1/2}$, where $\Delta_{\rm ss}$ is the density at which the gas begins to self-shield, and $\Delta \sim 10 \times \Delta_{\rm ss}$ is the density of the relevant high-column density systems (see below).

In order to allow the gas to dynamically relax, we turn on an optically thin Haardt & Madau (2012) background at $z = 9$, roughly corresponding to the mid-point of reionization (Hinshaw et al. 2013). We caution however that the dynamical relaxation of the baryons depends on their poorly constrained thermal histories. We use the temperature, density, velocity and halo fields at $z = 7$, mapped on to a fixed 1024^3 grid. Below we describe our prescription for generating the corresponding neutral hydrogen maps.

We take the mean photoionization rate inside H II patches (in units of 10^{-12} s^{-1}), $\langle\Gamma_{12}\rangle_{\rm H\,II}$, as our free parameter in computing the opacity from the local, cosmic H II region in which the galaxy is embedded, $\tau_{\rm H\,II}$:

$$\tau_{\rm H\,II}(\langle\Gamma_{12}\rangle_{\rm H\,II}) = \int_{R_{\rm min}}^{R_{\rm H\,II}} \frac{c\,{\rm d}t}{{\rm d}z} n_{\rm H} x_{\rm H\,I} \sigma_\alpha, \quad (3)$$

where $n_{\rm H} = \Delta\bar{n}_{\rm H}$ is the cell's hydrogen number density, σ_α is the Lyα cross-section at a given frequency (taking into account peculiar motions of the gas), and the neutral fraction, $x_{\rm H\,I}$, is computed according to equation (5) below. As we wish to avoid modelling the complexities of the interstellar and circumgalactic media, we start the optical depth integral at a (somewhat arbitrary) distance $R_{\rm min}$=0.16 cMpc away from the halo centre, in order to match the choice in Bolton & Haehnelt (2013) for a more direct comparison. The interstellar and circumgalactic media affect the line shape of the Lyα line as it emerges from a galaxy. By varying the line shape, we address uncertainties associated with scattering process on these smaller scales. We stop the integration of equation (3) at a distance of $R_{\rm H\,II}$ from the galaxy, corresponding to the size of a cosmic H II patch at a given stage in reionization, $Q_{\rm H\,II}$. Our large-scale reionization simulations provide the distribution of $R_{\rm H\,II}$ values, sampled according to the Monte Carlo procedure described in Section 2.1.

As the clustering of local sources can be important, we construct the local photoionization field overdensity, $\Delta_\Gamma(\boldsymbol{x}) \equiv \Gamma_{12}(\boldsymbol{x})/\langle\Gamma_{12}\rangle_{\rm H\,II}$, where the local ionization rate, $\Gamma_{12}(\boldsymbol{x})$, is computed using a simple, optically thin r^{-2} attenuation profile, and assuming that the galaxy's emissivity of ionizing photons is proportional to its total halo mass (e.g. Mesinger & Dijkstra 2008):

$$\Gamma_{12}(\boldsymbol{x}) \propto \sum_i \frac{M_{\rm halo,\,i}}{|\boldsymbol{x} - \boldsymbol{x}_i|^2}\, {\rm e}^{-|\boldsymbol{x}-\boldsymbol{x}_i|/\lambda_{\rm mfp}}. \quad (4)$$

Note that the proportionality constant is set by $\langle\Gamma_{12}\rangle_{\rm H\,II}$. Here $\boldsymbol{x}_i$ is the location of halo i, $M_{\rm halo,\,i}$ its mass, and $\lambda_{\rm mfp}$ the mean free path of ionizing photons. We take $\lambda_{\rm mfp} = 14$ Mpc, corresponding to the radius of our entire simulation box, which is also in agreement with typical sizes of H II regions near the end of reionization (e.g. Sobacchi & Mesinger 2014). For computational efficiency, the Δ_Γ field is computed on a lower resolution, 256^3 grid. We stress that this is a conservative[3] choice, likely *overestimating the importance of self-shielded systems*, as the flux enhancements near galaxies (where DLAs reside) are smoothed over using such a relatively coarse grid.

[3] Throughout this work, we use 'conservative' to indicate assumptions which weaken the derived constraints on reionization.

2.2.1 Self-shielding prescription

Assuming photoionization equilibrium, we calculate the neutral fraction at a given density

$$x_{\rm H\,I}\Gamma_{12,\rm ss} = \chi_{\rm He\,II}\, n_{\rm H}\, (1 - x_{\rm H\,I})^2\, \alpha_{\rm B}(T), \quad (5)$$

where $\alpha_{\rm B}(T)$ is the case B recombination coefficient (e.g. Spitzer 1978) for gas at temperature T, and $\chi_{\rm He\,II} = 1.08$ accounts for singly ionized helium. Since our simulations do not include radiative transfer (RT), we use the empirical fit from the RT simulations of Rahmati et al. (2013), in order to account for the self-shielding of the gas based on its local overdensity, Δ:

$$\frac{\Gamma_{12,\rm ss}}{\Gamma_{12}} = 0.98 \times \left[1 + \left(\frac{\Delta}{\Delta_{\rm ss}}\right)^{1.64}\right]^{-2.28} + 0.02 \times \left[1 + \frac{\Delta}{\Delta_{\rm ss}}\right]^{-0.84}, \quad (6)$$

where $\Delta_{\rm ss}$ is the overdensity above which the gas begins to self-shield (Schaye 2001):

$$\Delta_{\rm ss} \approx 15 \left(\frac{\Gamma_{12}}{0.1}\right)^{2/3} \left(\frac{T}{10^4\ {\rm K}}\right)^{-0.13} \left(\frac{1+z}{7}\right)^{-3}, \quad (7)$$

where the pre-factor is computed also assuming a soft, stellar-dominated UVB with an energy index of $\alpha = 5$. We caution that details of the dynamic relaxation of the gas could impact some of these results at $z \sim 7$. The thermal history of the high-redshift Universe is poorly constrained, though simple scaling relations based on local galaxies (e.g. Mineo, Gilfanov & Sunyaev 2012) suggest that X-rays can already heat the IGM to thousands of Kelvin, before the bulk of reionization (Furlanetto 2006; McQuinn & O'Leary 2012; Mesinger, Ferrara & Spiegel 2013).

In Fig. 4, we show the resulting distributions of opacities from the ionized IGM ($Q_{\rm H\,II} = 1$). Comparing these opacities to the analogous ones sourced by the large-scale reionization morphology, shown in Fig. 2, we see that in general the absorption profile from self-shielded systems is steeper than that from the neutral IGM (e.g. Miralda-Escude 1998; Mesinger & Furlanetto 2008a). Moreover, when making reionization constraints it is common to assume that all flux redwards of the systemic redshift is fully transmitted through the ionized IGM. However, in Fig. 4 we see that there is strong absorption from proximate infalling gas at $\Delta v \lesssim 100$–$200\ {\rm km\,s^{-1}}$, even if $Q_{\rm H\,II} = 1$ and $\langle\Gamma_{12}\rangle_{\rm H\,II}$ is high (as one might expect at $z \sim 6$; see also e.g. Dijkstra et al. 2011). One must account for this absorption (present post-reionization) when computing the *relative* difference in Lyα transmission between $z \sim 6$ and 7 samples.

It is very important to note that gas only *begins* to self-shield at $\Delta \sim \Delta_{\rm ss}$, and is still mostly ionized at these densities. Strong damping wing absorption requires neutral fractions close to unity, i.e. DLAs rather than Lyman limit systems (LLSs). Radiative transfer simulations (McQuinn, Oh & Faucher-Giguère 2011; Rahmati et al. 2013) show that gas becomes mostly neutral well beyond this threshold, requiring $\Delta \gtrsim 10 \times \Delta_{\rm ss}$. Therefore, assuming that systems with $\Delta > \Delta_{\rm ss}$ are fully neutral, as was done in Bolton & Haehnelt (2013), can dramatically overestimate the opacity of the ionized IGM (see also Keating et al. 2014).

This is shown explicitly in Fig. 5. In the left and centre panels, we show slices through the neutral fraction field, computed according to equations (5)–(7). The left-hand panel assumes $\langle\Gamma_{12}\rangle_{\rm H\,II} = 0.1$, while the centre one assumes $\langle\Gamma_{12}\rangle_{\rm H\,II} = 0.01$. As we shall see below, the latter is a conservatively low choice of $\langle\Gamma_{12}\rangle_{\rm H\,II}$, thus maximizing the importance of self-shielded systems. In the right-hand

Downloaded from https://academic.oup.com/mnras/article-abstract/446/1/566/1322451 by guest on 03 June 2020

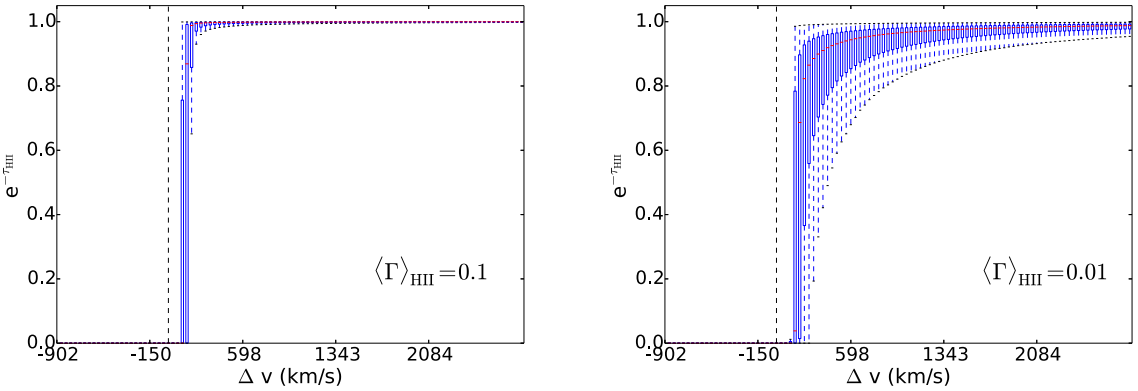

Figure 4. Distributions of the damping wing transmission from the ionized IGM ($Q_{\rm H\,II} = 1$), with $\langle\Gamma_{12}\rangle_{\rm H\,II}$=0.1 (0.01) shown on the left (right). Red lines correspond to the median profile, while boxes/whiskers enclose the first two quartiles of the distribution.

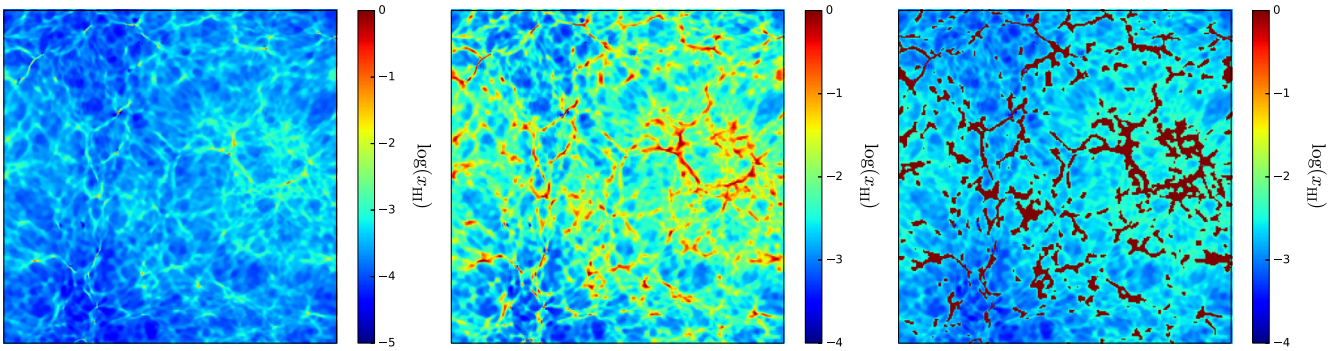

Figure 5. Maps of the neutral fraction (22 Mpc across and 21 kpc thick). The first two panels are generated using our fiducial self-shielding prescription, described in the text, and assuming $\langle\Gamma_{12}\rangle_{\rm H\,II} = 0.1$ (left-hand panel) and 0.01 (middle panel). Like the middle panel, the right-hand panel also corresponds to $\langle\Gamma_{12}\rangle_{\rm H\,II} = 0.01$, but instead is computed using the approximation that systems with $\Delta > \Delta_{\rm ss}$ are fully neutral (cf. bottom-right panel of fig. 1 in Bolton & Haehnelt 2013).

panel, we also assume $\langle\Gamma_{12}\rangle_{\rm H\,II} = 0.01$, but instead compute the neutral fraction with the approximation used in Bolton & Haehnelt (2013): that gas with $\Delta \geq \Delta_{\rm ss}$ is *fully* neutral. We see that this approximation results in a dramatic discontinuity in the neutral fraction map at the edges of filaments (cf. bottom-right panel of fig. 1 in Bolton & Haehnelt 2013; note that the discontinuity is smoothed over by averaging over a fixed step size when creating their fig. 3).

This is further quantified in Fig. 6, where we show the cumulative distribution functions of the transmission, $\exp[-\tau_{\rm H\,II}]$, again computed at a rest-frame velocity offset of $\Delta v = 200\,{\rm km\,s^{-1}}$. The red dotted curve is computed according to our fiducial prescription above assuming $\langle\Gamma_{12}\rangle_{\rm H\,II} = 0.01$, corresponding to the middle panel of Fig. 5. Even for such a low $\langle\Gamma_{12}\rangle_{\rm H\,II}$, the attenuation along most sightlines is modest, with the average transmission at $\Delta v = 200\,{\rm km\,s^{-1}}$ being $\exp[-\tau_{\rm H\,II}] \approx 0.8$. There is a high opacity tail corresponding to ∼15 per cent of LOSs which encounter high-column density systems. On the other hand, when the opacity is computed with the previous simplification of fully neutral gas at $\Delta \geq \Delta_{\rm ss}$ (*blue dot–dashed curve*), the transmission drops dramatically. In this case, the mean transmission at $\Delta v = 200\,{\rm km\,s^{-1}}$ is $\exp[-\tau_{\rm H\,II}] \approx 0.2$, and the sightline scatter is very broad.

It is worthwhile also to highlight the qualitative differences between the cumulative distribution functions in Figs 3 and 6. Namely, the opacities sourced from the H II regions (i.e. self-shielded systems) are relatively bimodal: either an LOS encounters a nearby high-column density system and the Lyα is strongly absorbed, or it does not and the attenuation is modest. On the other hand, opacities sourced from the large-scale reionization morphology are unimodal, as the damping wings from the cosmic neutral patches are smoother functions of wavelength and so even distant patches impart a modest attenuation. This is in contradiction to recently popularized Bayesian studies (e.g. Treu et al. 2012, 2013; Pentericci et al. 2014; Tilvi et al. 2014) which use an empirical 'on/off' model (called 'patchy') as a proxy for reionization attenuation.

2.2.2 *Biases in the density and ionization fields*

Galaxies reside in biased locations of both the density and ionizing background fields. In terms of the resulting IGM opacity, these two biases act in opposite directions. Biased locations of the density field imply more surrounding structure, capable of hosting high-column density systems. On the other hand, biased locations in the photoionization field imply a stronger overdensity criterion for self-shielding (i.e. higher value of $\Delta_{\rm ss}$ in equation 7 resulting from a higher Γ_{12}).

We briefly show the impact of these biases on the Lyα transmission by comparing the red-dotted and green-dashed lines in Fig. 6. The former is constructed with LOSs originating from haloes, while the latter is constructed from LOSs originating from random locations in the simulation box. We see that in this case, the density bias 'wins': although the mean transmissions are comparable, sightlines originating at random locations are understandably far less likely to

Downloaded from https://academic.oup.com/mnras/article-abstract/446/1/566/1322451 by guest on 03 June 2020

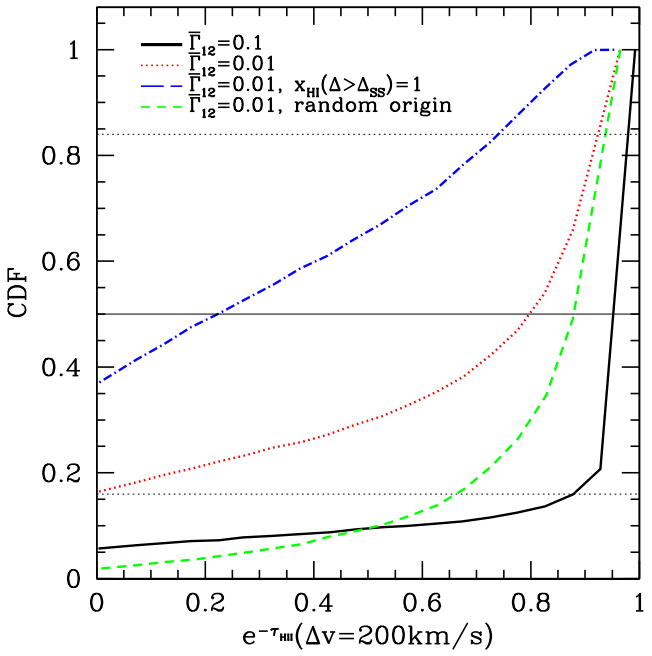

Figure 6. Fraction of sightlines having H II transmissions less than $\exp[-\tau_{\rm H\,II}]$, evaluated at $\Delta v = 200\,{\rm km\,s^{-1}}$ redwards of the galaxy's systemic redshift. The solid black curve corresponds to $\langle\Gamma_{12}\rangle_{\rm H\,II}$=0.1, while the others correspond to $\langle\Gamma_{12}\rangle_{\rm H\,II}$=0.01. The dotted-red curve is computed using our fiducial prescription (equations 5–7), while the blue dot–dashed curve is computed using the approximation that systems with $\Delta > \Delta_{\rm ss}$ are fully neutral. The green-dashed curve is also computed using our fiducial prescription, but with sightlines originating at random locations in the IGM, instead of halo centres.

encounter nearby self-shielded systems. The increase in the local photoionization rate is unable to counter the higher incidence of structures near galaxies. However, we again caution that we underestimate the fluctuations in the local photoionization rate, since (i) the photoionization overdensity field, Δ_Γ, is computed on a relatively coarse, 256^3 grid; and (ii) our ENZO box is too small to capture large-scale fluctuations in Γ_{12} (e.g. Crociani et al. 2011).

2.3 Combining the IGM opacity from ionized and neutral cosmic patches

As described in the previous sections, our approach splits the total optical depth into a component sourced by the large-scale reionization morphology, $\tau_{\rm reion}$, and from the residual neutral hydrogen inside the cosmic H II patches surrounding galaxies, $\tau_{\rm H\,II}$, so that the total Lyα optical depth is:

$$\tau(Q_{\rm H\,II}, \langle\Gamma_{12}\rangle_{\rm H\,II}) = \tau_{\rm reion} + \tau_{\rm H\,II} = \int_{R_{\rm H\,II}}^{R_{\rm max}} d\tau_{\rm reion} + \int_{R_{\rm min}}^{R_{\rm H\,II}} {\rm d}\tau_{\rm H\,II}. \quad (8)$$

The two sources of opacity are 'glued-together' using the limit of integration, $R_{\rm H\,II}$, drawn from the distribution of sizes of cosmic H II regions in our reionization simulations at a given value of $Q_{\rm H\,II}$. In other words, for distances less than $R_{\rm H\,II}$, the sightline's opacity is fully determined by the hydrodynamic simulation ($\tau_{\rm H\,II}$), while at greater distances it is fully determined by the reionization simulation ($\tau_{\rm reion}$). Hence, $\tau_{\rm reion}$ is sourced by order unity fluctuations of the large-scale reionization field, while $\tau_{\rm H\,II}$ is sourced by the incidence rate of self-shielded, high-column density systems (though our formalism for $\tau_{\rm H\,II}$ accounts for the absorption by *all* of the gas inside the local H II region, not just from the self-shielded systems; see Fig. 1).

2.4 The intrinsic Lyα emission line

Having constructed a data base of optical depth profiles from *both* reionization, $\tau_{\rm reion}$, *and* the local H II region, $\tau_{\rm H\,II}$, we now need the intrinsic Lyα line, $J(\nu)$, emerging from the galaxy's interstellar and circumgalactic media (which in our case corresponds to distances within 0.16 cMpc of the galaxy, as mentioned above). The total transmission, $T_{\rm IGM}$, is then an integral over the intrinsic line:

$$T_{\rm IGM} = \int {\rm d}\nu J(\nu) \exp[-\tau_{\rm reion}(\nu) - \tau_{\rm H\,II}(\nu)], \quad (9)$$

where $J(\nu)$ is normalized to integrate to unity.

Modelling $J(\nu)$ is beyond the scope of this work. Hence we just assume simple Gaussian profiles, centred at $\Delta v = 0$, 200, 400 km s^{-1} redwards of the systemic redshift, with an rms width of 100 km s^{-1}, roughly corresponding to the circular velocities of the host haloes (e.g. Barkana & Loeb 2004). In reality, the profile of $J(\nu)$ is much more complicated, likely involving radiative transfer through outflowing material (see for example Dijkstra et al. 2011; Dijkstra 2014 and references therein). However, our relatively narrow Gaussians sample the range of Lyα emission observed in low-z LAEs (e.g. Steidel et al. 2010; Shibuya et al. 2014). By sampling both the low and high ends of the likely systemic offset of the Lyα profile, we bracket the expected impact of $J(\nu)$ on our results. As we shall see below, the choice of $J(\nu)$ does not have a large impact on $Q_{\rm H\,II}$ constraints (unless there is *evolution* in $J(\nu)$ from $z = 6 \rightarrow 7$)[4] though it does have a modest impact on $\langle\Gamma_{12}\rangle_{\rm H\,II}$ constraints.

3 RESULTS

3.1 Total IGM transmission

In Fig. 7, we plot the sightline-averaged ratio of IGM Lyα transmission (equation 9) at $z = 7$ and 6: $\langle T_{\rm IGM,\,z7}/T_{\rm IGM,\,z6}\rangle$. $T_{\rm IGM,\,z6}$ is computed assuming $(Q_{\rm H\,II}, \langle\Gamma_{12}\rangle_{\rm H\,II})_{z6} = (1, 0.2)$, and neglecting redshift evolution of other quantities (i.e. $\langle T_{\rm IGM,\,z7}/T_{\rm IGM,\,z6}\rangle \equiv 1$ in the top-right corner of the parameter space; see below for some motivation of this conservative choice). The left (right) panel assumes an intrinsic emission profile, $J(\nu)$, centred at $\Delta v = 200$ (400) km s^{-1}.

From the modest inclination of the isocontours over the upper half of parameter space in Fig. 7, we see that the transmission ratio is more sensitive to $Q_{\rm H\,II}$ than $\langle\Gamma_{12}\rangle_{\rm H\,II}$, despite our conservative assumptions mentioned above. Proximate self-shielded systems only impact the average transmission when $\langle\Gamma_{12}\rangle_{\rm H\,II} \lesssim 0.02$. The transmission is even less sensitive to $\langle\Gamma_{12}\rangle_{\rm H\,II}$ if the intrinsic Lyα line, $J(\nu)$, has a larger systemic velocity offset (i.e. the right-hand panel of Fig. 7). As already mentioned, this is due to the fact that self-shielded systems generally have absorption profiles which are steeper with wavelength than the neutral IGM (e.g. Miralda-Escude 1998; McQuinn et al. 2008; Mesinger & Furlanetto 2008a). Therefore if the

[4] The line profile might indeed evolve with redshift. For example, Jones, Stark & Ellis (2012) show that the covering factor of low-ionization absorbers (which trace HI) decreases from $z = 3 \rightarrow 4$ in LBGs. They argue that it is in fact the covering factor that is regulating Lyα escape, which could imply a redshift evolution of $J(\nu)$.

Downloaded from https://academic.oup.com/mnras/article-abstract/446/1/566/1322451 by guest on 03 June 2020

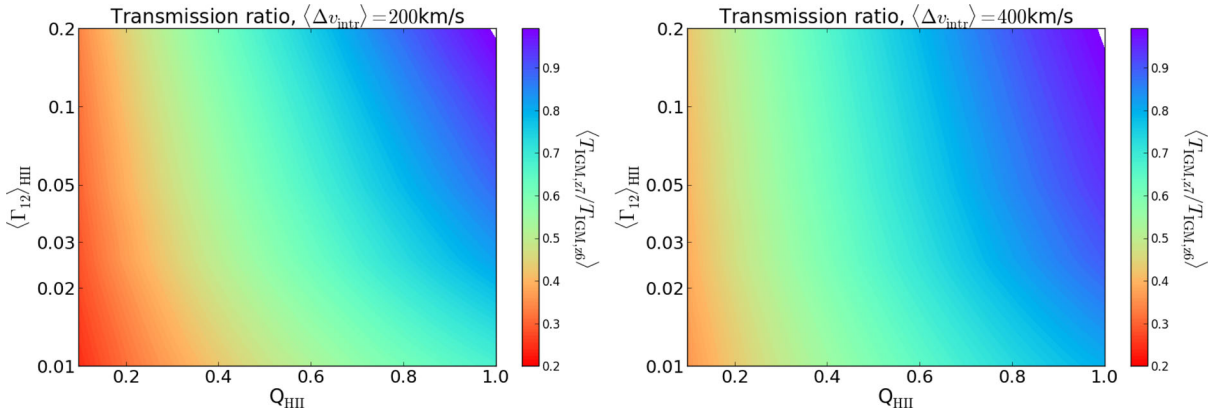

Figure 7. Sightline-averaged ratio of IGM Lyα transmission (equation 9) at $z = 6$ and 7: $\langle T_{\rm IGM,\,z7}/T_{\rm IGM,\,z6} \rangle$. The axes correspond to our $z = 7$ model parameters: $(Q_{\rm H\,II}, \langle \Gamma_{12} \rangle_{\rm H\,II})_{z7}$. $T_{\rm IGM,\,z6}$ is computed assuming $(Q_{\rm H\,II}, \langle \Gamma_{12} \rangle_{\rm H\,II})_{z6} = (1, 0.2)$, and neglecting redshift evolution of other quantities (i.e. by construction $T_{\rm IGM,\,z7}/T_{\rm IGM,\,z6} = 1$ in the top-right corner of the panels). The left (right) panel assumes an intrinsic emission profile, $J(\nu)$, centred at $\Delta v = 200$ (400) km s^{-1}.

intrinsic Lyα emission has a significant contribution far redwards of the systemic redshift, it will be even less sensitive to self-shielded systems than reionization.

It is also interesting to note that even for the largest $z = 6 \rightarrow 7$ evolution considered, $(Q_{\rm H\,II}, \langle \Gamma_{12} \rangle_{\rm H\,II})_{z7} \approx (0.1, 0.01)$,[5] the transmission ratio is still not very small, $\langle T_{\rm IGM,\,z7}/T_{\rm IGM,\,z6} \rangle = 0.2$–$0.4$. This is driven by the emission redwards of the systemic velocity (physically motivated by radiative transfer through outflows; e.g. Verhamme et al. 2008), some of which is transmitted even through a neutral IGM.

We stress that up to now, our results have not made use of any observations. Fig. 7 shows our model predictions, which can be used to interpret evolving observational data sets, as we illustrate below.

3.2 Lyman alpha fractions

We now turn to modelling the redshift evolution of the Lyα fraction. For this, we need the distribution of REWs at $z \approx 6$, REW$_{z6}$. Our $z \approx 6$ galaxy sample consists of 56 colour-selected galaxies with Very Large Telescope spectroscopy, and is a collection of past and ongoing programmes (Fontana et al. 2010; Pentericci et al. 2011, 2014, Vanzella et al. in preparation). The integration times span the range between 5 and 18 h on target. The sample does not include galaxies for which there is no spectroscopic redshift confirmation (either from a Lyα line or from the Lyα break). Since such null detections are included when presenting $z \approx 7$ fractions, we expect our $z \approx 6$ spectroscopic sample to overpredict the $z = 6 \rightarrow 7$ drop. Hence, we add four additional REW=0 Å galaxies, so that our fiducial $z \approx 6$ fractions match those recently published in Schenker et al. (2014), allowing us to compare against their $z \approx 7$ results. We note that our main predictions of the $z = 6$ and 7 Lyα fraction ratios in Fig. 9 are unaffected by this overall normalization, depending only on the REW$_{z6} > 25$ Å distribution of UV faint galaxies.

As already noted (e.g. Stark et al. 2010; Ono et al. 2012), the most dramatic change in the Lyα fraction from $z = 6 \rightarrow 7$ is driven by UV faint galaxies ($M_{\rm UV} \gtrsim -20.25$). In Fig. 8, we plot the $z \approx 7$ Lyα fraction, $f_{{\rm Ly}\alpha}(z \approx 7)$, defined as the fraction of UV faint galaxies with REWs greater than 25 Å. This is computed by Monte Carlo sampling the REW compilation of $z \approx 6$ galaxies, REW$_{z6}$. Each sightline, i, at $z = 7$ is then assigned a REW$^i_{z7}$ = REW$^i_{z6} \times T^i_{\rm IGM,z7}/T^i_{\rm IGM,z6}$, and we compute the resulting fraction with REW$_{z7} > 25$ Å for each point in our $(Q_{\rm H\,II}, \langle \Gamma_{12} \rangle_{\rm H\,II})_{z7}$ parameter space.

We denote the observed estimates of $f_{{\rm Ly}\alpha}(z = 7)$ from Schenker et al. (2014) (*thick solid lines*), as well as the 1 (2) σ isocontours with thin dashed (dotted) lines. We stress that this analysis assumes that the change in IGM transmission is entirely driving the change in Lyα fraction. For simplicity, we do not correlate the REW with the host halo mass. This is reasonable, as our host haloes only span a factor of few in mass and the halo bias (i.e. local environment) is relatively constant over this mass range. Moreover, we neglect cosmic variance in the reionization morphology, which Taylor & Lidz (2014) showed can impact the interpretation of previous observational samples. This choice was made for several reasons: (i) new samples (e.g. Pentericci et al. 2014; Schenker et al. 2014) probe much larger volumes, better sampling reionization morphology (especially during the relevant advanced stages); (ii) calculations for the newer samples in Pentericci et al. (2014) already showed EoR cosmic variance to be small, especially when computed redwards of the systemic redshift, as relevant for most of the intrinsic Lyα line profile; (iii) we wish to present general results which can be used to easily interpret new data.

If the intrinsic Lyα line has a large systemic redshift, $\Delta v = 400$ km s^{-1} (*right-hand panel*), it is difficult for the IGM to significantly impact the transmission, as most of the emission lies far out on the damping wing tail of the absorption. Hence, a very large neutral fraction is required for even a modest change in the Lyα fraction.

On the other hand, under the more reasonable assumption that the intrinsic line is less redshifted, $\Delta v = 200$ km s^{-1} (*centre panel*), we see that $Q_{\rm H\,II}(z = 7) \lesssim 0.25$[6] is required to be consistent with

[5] A fully neutral (or close to fully neutral) universe would result in lower transmission. We do not however explore such tiny values of $Q_{\rm H\,II}$ since (i) our approach does not model tiny, sub-grid H II regions prevalent in the very first stages of the EoR; (ii) the implied sharp reionization ($\Delta z_{\rm re} \approx 1$) is extremely unlikely.

[6] For simplicity, it is common in the literature to assume $T_{\rm IGM,\,z6} = 1$ redwards of the systemic redshift. However, resonant absorption in infalling

Downloaded from https://academic.oup.com/mnras/article-abstract/446/1/566/1322451 by guest on 03 June 2020

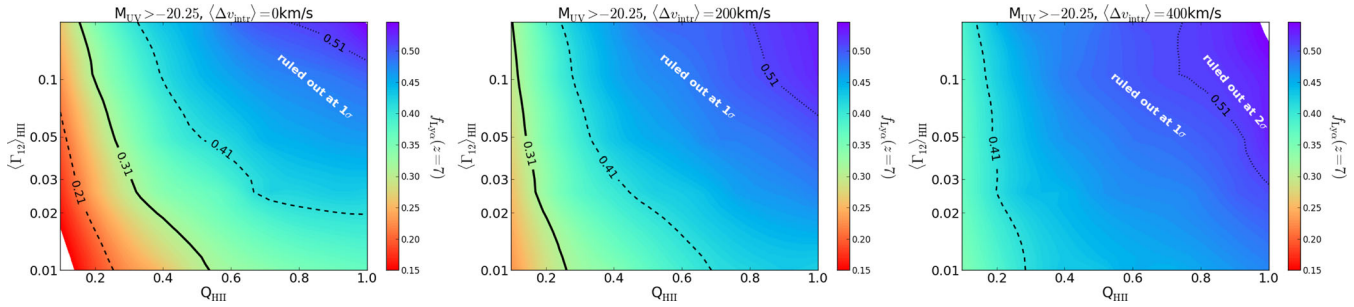

Figure 8. Fraction of UV faint galaxies ($M_{\rm UV} \gtrsim -20.25$) with REW > 25 Å at $z = 7$, assuming the intrinsic REW distribution is the same as at $z = 6$. We denote the observed estimates of $f_{\rm Ly\alpha}(z = 7)$ from Schenker et al. (2014) (thick solid lines), as well as the 1 (2) σ isocontours with thin dashed (dotted) lines. The left, centre, right panels assume an intrinsic emission profile, $J(v)$, centred at $\Delta v = 0$, 200, 400 km s^{-1}, respectively.

observations at 1σ, barring evolution in $\langle\Gamma_{12}\rangle_{\rm H\,II}$ (cf. the top axis of the panel). Conversely, even $\langle\Gamma_{12}\rangle_{\rm H\,II}(z = 7) \sim 0.01$ is not low enough to be consistent with observations at 1σ, if the IGM is ionized at $z = 7$ (cf. the right axis of the panel). As we shall see below, the IGM properties are highly unlikely to evolve so dramatically over such a narrow redshift interval.

On the other hand, allowing for a *joint* evolution in IGM properties relaxes somewhat the mild tension with data. For example, $Q_{\rm H\,II} \lesssim 0.5$ and $\langle\Gamma_{12}\rangle_{\rm H\,II} \lesssim 0.02$ are allowed at 1σ in the middle panel.

The left-hand panel shows Lyα fractions under the extreme assumption that there is no offset between the intrinsic Lyα line and the systemic redshift of the galaxy. This model is inconsistent with observations at lower redshifts (e.g. Steidel et al. 2010; Shibuya et al. 2014). It results in only a few per cent of the Lyα line being transmitted far out on the red wing of the line, even at $z \approx 6$, as infalling gas on average resonantly absorbs the emission at $\Delta v \approx 100$–200 km s^{-1} redwards of the systemic redshift (cf. the left-hand panel of Fig. 4). However, it serves to illustrate that for the majority of 'reasonable' parameter space (i.e. the upper right quadrant), the Lyα fractions are only mildly different from the more reasonable $\Delta v = 200$ km s^{-1} model. This is due to the fact that we are normalizing the Lyα fractions to the same value at $(Q_{\rm H\,II}, \langle\Gamma_{12}\rangle_{\rm H\,II}) = (1, 0.2)$, our fiducial choice for $z \approx 6$.

3.3 Evolution of the Lyman alpha fractions

The *evolution* of the Lyα emission is better understood as a *ratio* of the Lyα fractions. In Fig. 9, we show the ratio of the $z \approx 7$ and 6 Lyα fractions for the UV faint galaxies: $f_{\rm Ly\alpha}(z \approx 7)/f_{\rm Ly\alpha}(z \approx 6)$. Here for simplicity, we only assume $\Delta v = 200$ km s^{-1} for the intrinsic Lyα emission.

Fig. 9 can be readily applied to interpret new observations. The ratios shown in the figure do not depend on the assumed normalization of the $z \approx 6$ REW PDF, nor on how the REW is distributed at low values REW < 25 Å (which is difficult to determine observationally), as these REW are already 'non-detections' by the definition of the Lyα fraction. It only depends on the shape of the $z \approx 6$ distribution at REW > 25 Å, as these are the galaxies that can move over from the 'detectable Lyα' category to the 'non-detectable Lyα' category, due to IGM evolution from $z \approx 6$ to 7.

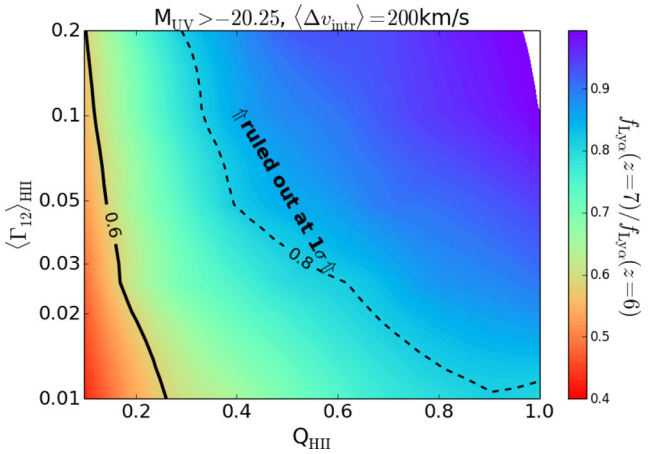

Figure 9. Ratio of $z \approx 7$ and 6 Lyα fractions, $f_{\rm Ly\alpha}(z = 7)/f_{\rm Ly\alpha}(z = 6)$, for the UV faint sample, $M_{\rm UV} > -20.25$, assuming $\Delta v = 200$ km s^{-1}. The black solid (dashed) curves corresponds to the best fit (1σ) from Schenker et al. (2014).

This ratio of Lyα fractions shows the $z = 6 \rightarrow 7$ evolution more explicitly. For our parameter space, the Lyα fraction physically cannot drop by more than a factor of $\sim$2. This is driven by objects with large values of REW$_{z6}$. The evolution of IGM properties (Fig. 7) is insufficient to suppress such high REWs to values of REW$_{z7} < 25$ Å. As we discuss below, more reasonable models lie in the upper right quadrant of parameter space; here the ratio of Lyα fractions only evolves by tens of per cent. Larger evolution of the Lyα fraction would be possible if the distribution of REW$_{z6}$ was more sharply peaked towards low values, REW$_{z6} \approx 25$ Å, again highlighting the need for larger, more robust galaxy samples.

We also show the 1σ observational uncertainty on the ratio of Lyα fractions, computed with standard error propagation, with the dashed curve. Unlike the observational uncertainty on $f_{\rm Ly\alpha}(z \approx 7)$ shown in Fig. 8, the uncertainty in $f_{\rm Ly\alpha}(z \approx 7)/f_{\rm Ly\alpha}(z \approx 6)$ includes the additional Poisson error in $f_{\rm Ly\alpha}(z \approx 6)$. The black solid (dashed) curves corresponds to the best fit (1σ) from Schenker et al. (2014)

material can attenuate intrinsic emission redwards of the systemic redshift, even without reionization or DLAs. Compared to such prior analysis, our more realistic treatment results in higher $T_{\rm IGM,\,z7}/T_{\rm IGM,\,z6}$ ratios, strengthening constraints on $Q_{\rm H\,II}$ (i.e. by making it more difficult for the IGM to produce a given drop in the Lyα fraction). This offsets the loosening of constraints from our new, feedback-limited reionization morphologies. Therefore, our derived constraints on $Q_{\rm H\,II}$ (assuming no $\langle\Gamma_{12}\rangle_{\rm H\,II}$ evolution), are not as different from previous ones, as would be expected from the discussion in Section 2.1.1. We also note that models in which outflows set the emerging Lyα line profile result in considerable line shifts, even for modest outflow velocities (e.g. Dijkstra et al. 2011). Hence the above distinction is less relevant for these models.

Downloaded from https://academic.oup.com/mnras/article-abstract/446/1/566/1322451 by guest on 03 June 2020

(see their fig. 9). All of the parameter space is consistent with observations at 2σ.[7]

One can also convert Fig. 9 to a likelihood and marginalize over one of the dimensions. Using a standard $e^{-\chi^2/2}$ estimator and adopting a uniform prior in $\log\langle\Gamma_{12}\rangle_{\rm H\,II}$, we obtain a marginalized 68 per cent confidence level of $Q_{\rm H\,II}(z \approx 7) \leq 0.6$. Future measurements could be used to motivate priors in either $\langle\Gamma_{12}\rangle_{\rm H\,II}$ or $Q_{\rm H\,II}$, further increasing the constraining power of this analysis.

3.4 What is 'reasonable' for the IGM at $z = 7$?

Our IGM parameter space, $(Q_{\rm H\,II}, \langle\Gamma_{12}\rangle_{\rm H\,II})_{z7}$, is conservatively broad. It would therefore be useful to estimate what evolution is 'physically reasonable', in order to (qualitatively) tighten constraints. We discuss this briefly below.

3.4.1 Reionization

The evolution of the final stages of reionization depends on the evolution of the sources (galaxies) and sinks (LLSs and more diffuse systems) of ionizing photons. The filling factor of H II regions depends on the source and sink terms as (e.g. Shapiro & Giroux 1987)

$$\frac{{\rm d}Q_{\rm H\,II}}{{\rm d}t} = \frac{\rm d}{{\rm d}t}[f_* f_{\rm esc} f_{\rm b} N_\gamma f_{\rm coll}] - \alpha_B n_{\rm b} C (1+z)^3 Q_{\rm H\,II}, \quad (10)$$

where N_γ is the number of ionizing photons per stellar baryon, $f_{\rm esc}$ is the fraction of UV ionizing photons that escape into the IGM, $f_\star$ is the fraction of galactic gas in stars, and $f_{\rm b}$ is the fraction of baryons inside the galaxy with respect to the cosmic mean $\Omega_{\rm b}/\Omega_{\rm m}$, $f_{\rm coll}$ is the fraction of mass collapsed into haloes, C is the gas clumping factor.

Estimating this evolution is intrinsically complicated, as these parameters have a dependence on time, space, and (for the source terms) halo mass. Usually, the simplification is made that $f_{\rm coll}$ evolves more rapidly than the other terms, and thus governs the evolution of reionization. One can construct an extreme model (maximizing ${\rm d}Q_{\rm H\,II}/{\rm dt}$), by assuming that reionization is driven by only galaxies inside the most massive, rapidly evolving haloes. If one uses $M_{\rm halo} \gtrsim 10^{11}\,{\rm M}_\odot$, roughly corresponding to the observed Lyman break galaxies (LBG) at high redshift (e.g. Dayal & Ferrara 2012), the resulting maximal evolution over $\Delta z \approx 1$ is $\Delta Q_{\rm H\,II} \lesssim 0.5$–$0.6$ (e.g. fig. 1 in Lidz et al. 2007). However, this model would require a 'tuned', rapid fall of the 'f' parameters of the source term in equation 10 at $z \sim 6$ in order counter the rapid rise in ${\rm d}f_{\rm coll}(M_{\rm min})/{\rm dt}$, so as to reproduce the observed flat emissivity evolution at $z \lesssim 5$ (e.g. Miralda-Escudé 2003; fig. 12 in Mesinger, McQuinn & Spergel 2012).

Furthermore, it is quite likely that the 'sinks' regulate the final stages of reionization. As H II regions grow, they become 'recombination-limited' (Furlanetto & Oh 2005), and an increasing fraction of the ionizing photons goes into balancing recombinations. In the late stages of reionization, this approximately translates to a rapid evolution in the clumping factor of the sink term in equation 10. The most complete study to date was done by Sobacchi & Mesinger (2014), who tracked the inhomogeneous evolution of sources and sinks via a sub-grid approach. Their 'FULL' model results in an evolution of $\Delta Q_{\rm H\,II} \lesssim 0.2$ over the final $\Delta z \approx 1$ of the EoR. However, it is likely that the late-stage evolution of $Q_{\rm H\,II}$ in Sobacchi & Mesinger (2014) is somewhat underestimated since: (i) they did not account for internal feedback, which can raise the value of $M_{\rm min}$, speeding up ${\rm d}f_{\rm coll}(M_{\rm min})/{\rm dt}$; (ii) the analytic formula used in the sub-grid density distribution (Miralda-Escudé, Haehnelt & Rees 2000) is inaccurate at very high densities (Bolton & Becker 2009) resulting in an underestimate of the emissivity evolution in the very late stages of (and following) reionization (McQuinn et al. 2011).

From the above, we conclude that over $\Delta z \approx 1$, it is reasonable to assume $\Delta Q_{\rm H\,II} \lesssim 0.2$–$0.5$. From the UV faint subsample in Figs 8 and 9, we see that this $\Delta Q_{\rm H\,II}$ requires $\langle\Gamma_{12}\rangle_{\rm H\,II} \lesssim 0.02$ to be consistent with $z = 7$ data at 1σ.

3.4.2 Photoionizing background

Can we say something about the value of $\langle\Gamma_{12}\rangle_{\rm H\,II}$ at $z = 7$? In Fig. 10, we show observational estimates of the photoionizing background at $z \leq 6$. The data does show tentative evidence for a slight evolution over $z = 5 \rightarrow 6$, though a much larger drop at $z = 6 \rightarrow 7$ would be required to be consistent with the Lyα fraction observations at 1σ, without evoking reionization (cf. right axis of Fig. 9).

From the theoretical side, any complete model of inhomogeneous reionization should also be able to self-consistently predict $\langle\Gamma_{12}\rangle_{\rm H\,II}$. Indeed, Sobacchi & Mesinger (2014) predict a change of $\langle\Gamma_{12}\rangle_{\rm H\,II}$ by

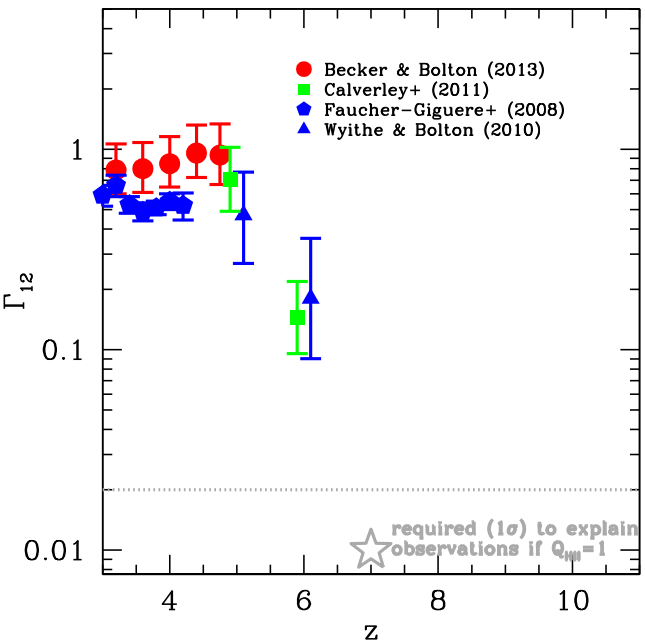

Figure 10. Estimates of the photoionizing background at $z \leq 6$ (in units of 10^{-12} s^{-1}). Points at $z = 5$, 6 are offset for clarity. Circles correspond to Becker & Bolton (2013), squares to Calverley et al. (2011), pentagons to Faucher-Giguère et al. (2008), and triangles to Wyithe & Bolton (2011). We also note with a grey star the maximum value of the photoionizing background at $z = 7$ required to be consistent at 1σ with the Lyα fraction, without evoking reionization. As seen in the text, the evolution in the Lyα fraction is relatively insensitive to the photoionizing background for values of $\gtrsim 0.02$. This transition from the Lyα fraction evolution being dominated by $Q_{\rm H\,II}$ to $\langle\Gamma_{12}\rangle_{\rm H\,II}$ is denoted by a horizontal dashed line.

[7] We do not compare with recent null detections at $z \approx 8$ (e.g. Treu et al. 2013; Schenker et al. 2014), as the resulting constraints depend heavily on understanding the systematic uncertainties and error bars on the null detection. For example, taken at face value from fig. 9 in Schenker et al. (2014), their claimed evolution of $z = 6 \rightarrow 8$ is inconsistent with IGM attenuation by more than 5σ, while non-Bayesian upper limits at $z \approx 8$ (e.g. Treu et al. 2013; Tilvi et al. 2014) are fully consistent with no evolution over this redshift range.

Downloaded from https://academic.oup.com/mnras/article-abstract/446/1/566/1322451 by guest on 03 June 2020

a factor of $\sim$2 over $\Delta z \approx 1$ in the final stages of reionization; however, as we mentioned above, the model of Sobacchi & Mesinger (2014) starts to break down post-reionization. A more rapid evolution could be achieved if the photoionizing background is dominated by quasars at $z \sim 7$ (Choudhury & Ferrara 2006), though empirical models disfavour a strong contribution from quasars at $z \gtrsim 4$ (Haardt & Madau 2012).

Further intuition can be gained if one simplifies the problem, studying the ionized IGM independently of the evolution of reionization. Using small-box, high-resolution radiative transfer simulations of the post-reionization IGM, McQuinn et al. (2011) show that a small change in the emissivity, ϵ, could drive a rapid change in the photoionizing background, with $\Gamma_{12} \propto \epsilon^{3.5-4.5}$ at $z \sim 6$. In this case, the factor $\sim$20 drop in $\langle\Gamma_{12}\rangle_{\rm H\,II}$ from $z = 6 \rightarrow 7$ required to explain the Lyα fraction without reionization, would still require ϵ to drop by a factor of a $\sim$ few (the additional evolution of the scaling relation between Γ_{12} and ϵ over this interval makes it difficult to present an accurate estimate), likely dropping to below the value required to reionize the Universe at $z \sim 7$. Hence, if one wishes to have such a low $\langle\Gamma_{12}\rangle_{\rm H\,II}(z = 7)$ and have reionization occur earlier at $z > 7$, the emissivity would likely have to evolve non-monotonically, with an additional, seemingly ad hoc population of ionizing sources at higher redshifts. Hence we conclude that it is implausible for an evolution in self-shielded systems to fully explain the Lyα fraction observations, without reionization, at the 1σ level.

4 CONCLUSIONS

Motivated by recent observational claims of a rapid drop at $z > 6$ in the Lyα fraction, we construct a tiered model for simulating the IGM attenuation. We combine large-scale seminumeric reionization simulations with moderate-scale hydrodynamic simulations of the ionized IGM. Thus, for the first time we account for the opacity of *both* patchy reionization *and* proximate, high-column density systems inside H II regions.

Using 5000 sightlines originating from $\sim 10^{11}\,{\rm M}_{\odot}$ haloes, we compute the average IGM transmission at $z = 7$ in a 2D parameter space consisting of (i) the filling factor of ionized regions, $Q_{\rm H\,II}$; and (ii) the average photoionization rate inside H II regions, $\langle\Gamma_{12}\rangle_{\rm H\,II}$. Our reionization morphologies are based on recent sub-grid models of UVB feedback on galaxies and an evolving recombination rate. The resulting morphologies are characterized by smaller H II regions, making it easier for reionization to explain the Lyα fraction evolution, compared to prior studies.

However, our models also include several, non-standard ingredients which act in the opposite direction, decreasing the predicted Lyα fraction evolution from $z = 6 \rightarrow 7$: (i) we use an intrinsic Lyα emission profile which is offset from the galaxy's systemic redshift (instead of just computing the opacity at the systemic redshift); (ii) we include the opacities of self-shielded systems also when computing the $z = 6$ transmission (instead of assuming zero opacity for all photons redwards of the systemic redshift); and (iii) we use a calibrated, continuous prescription for self-shielding inside H II regions (instead of a step-function transition at a given density threshold).

Taken separately, extreme evolution over $z = 6 \rightarrow 7$ in either reionization [$Q_{\rm H\,II}(z \approx 7) \lesssim 0.3$] or the photoionizing background [$\langle\Gamma_{12}\rangle_{\rm H\,II}(z \approx 7) < 0.01$] is required to be consistent with observations at the 1σ level. Assuming a joint evolution of IGM properties allows somewhat more reasonable models to be consistent at 1σ with data. Marginalizing over a uniform prior in $\log\langle\Gamma_{12}\rangle_{\rm H\,II}$, we obtain the constraint $Q_{\rm H\,II}(z \approx 7) \lesssim 0.6$ (1σ). We caution however that all of our parameter space is consistent with observations at 2σ, motivating larger galaxy samples.

Given our sample of $z \approx 6$ REWs, we predict that the Lyα fraction cannot drop by more than a factor of $\sim$2 with IGM attenuation alone, even for ionized fractions as low as $Q_{\rm H\,II} \gtrsim 0.1$. A greater change in the Lyα fraction would require some contribution from evolving galaxy properties (e.g. Jones et al. 2012; Dijkstra et al. 2014).

We also note that the attenuation in our patchy reionization models has a unimodal distribution over various sightlines (as already noted in prior Lyα emitter reionization studies; e.g. McQuinn et al. 2007; Mesinger & Furlanetto 2008b). This is in contradiction to recent Bayesian analyses (e.g. Treu et al. 2012, 2013; Pentericci et al. 2014; Tilvi et al. 2014) which use an empirical 'on/off' model (dubbed 'patchy') as a proxy for inhomogeneous reionization. In fact the damping wings from the cosmic neutral patches are smooth functions of wavelength and so even distant patches impart some attenuation. In contrast, the attenuation from the *ionized* IGM, i.e. self-shielded systems, is relatively more an 'on/off' process: a LOS either encounters a nearby high-column density system and the Lyα is strongly absorbed, or it does not and the attenuation is modest. This behaviour motivates the use of more physical models for the change in IGM transmission.

ACKNOWLEDGEMENTS

We thank J. Bolton for comments on a draft version of this manuscript. We thank the Italian SuperComputing Resource Allocation (ISCRA) for computational resources (proposal LAE_STAT).

REFERENCES

Barkana R., Loeb A., 2004, ApJ, 609, 474
Becker G. D., Bolton J. S., 2013, MNRAS, 436, 1023
Bolton J. S., Becker G. D., 2009, MNRAS, 398, L26
Bolton J. S., Haehnelt M. G., 2013, MNRAS, 429, 1695
Calverley A. P., Becker G. D., Haehnelt M. G., Bolton J. S., 2011, MNRAS, 412, 2543
Caruana J., Bunker A. J., Wilkins S. M., Stanway E. R., Lorenzoni S., Jarvis M. J., Ebert H., 2014, MNRAS, 443, 2831
Choudhury T. R., Ferrara A., 2006, MNRAS, 371, L55
Crociani D., Mesinger A., Moscardini L., Furlanetto S., 2011, MNRAS, 411, 289
Dayal P., Ferrara A., 2012, MNRAS, 421, 2568
Dijkstra M., 2014, preprint (arXiv:1406.7292)
Dijkstra M., Mesinger A., Wyithe J. S. B., 2011, MNRAS, 414, 2139
Dijkstra M., Wyithe S., Haiman Z., Mesinger A., Pentericci L., 2014, MNRAS, 440, 3309
Efstathiou G., 1992, MNRAS, 256, 43P
Fan X. et al., 2006, AJ, 132, 117
Faucher-Giguère C.-A., Lidz A., Hernquist L., Zaldarriaga M., 2008, ApJ, 688, 85
Fontana A. et al., 2010, ApJ, 725, L205
Furlanetto S. R., 2006, MNRAS, 371, 867
Furlanetto S. R., Oh S. P., 2005, MNRAS, 363, 1031
Furlanetto S. R., Zaldarriaga M., Hernquist L., 2004, ApJ, 613, 1
Furlanetto S. R., Zaldarriaga M., Hernquist L., 2006, MNRAS, 365, 1012
Haardt F., Madau P., 2012, ApJ, 746, 125
Haiman Z., Spaans M., 1999, ApJ, 518, 138
Hinshaw G. et al., 2013, ApJS, 208, 19
Hui L., Gnedin N. Y., 1997, MNRAS, 292, 27
Iliev I. T., Shapiro P. R., McDonald P., Mellema G., Pen U.-L., 2008, MNRAS, 391, 63
Iliev I. T., Mellema G., Ahn K., Shapiro P. R., Mao Y., Pen U.-L., 2014, MNRAS, 439, 725

Downloaded from https://academic.oup.com/mnras/article-abstract/446/1/566/1322451 by guest on 03 June 2020

Jensen H., Laursen P., Mellema G., Iliev I. T., Sommer-Larsen J., Shapiro P. R., 2013, MNRAS, 428, 1366
Jones T., Stark D. P., Ellis R. S., 2012, ApJ, 751, 51
Keating L. C., Haehnelt M. G., Becker G. D., Bolton J. S., 2014, MNRAS, 438, 1820
Lidz A., McQuinn M., Zaldarriaga M., Hernquist L., Dutta S., 2007, ApJ, 670, 39
McQuinn M., O'Leary R. M., 2012, ApJ, 760, 3
McQuinn M., Hernquist L., Zaldarriaga M., Dutta S., 2007, MNRAS, 381, 75
McQuinn M., Lidz A., Zaldarriaga M., Hernquist L., Dutta S., 2008, MNRAS, 388, 1101
McQuinn M., Oh S. P., Faucher-Giguère C.-A., 2011, ApJ, 743, 82
Mesinger A., Dijkstra M., 2008, MNRAS, 390, 1071
Mesinger A., Furlanetto S., 2007, ApJ, 669, 663
Mesinger A., Furlanetto S. R., 2008a, MNRAS, 385, 1348
Mesinger A., Furlanetto S. R., 2008b, MNRAS, 386, 1990
Mesinger A., Furlanetto S., Cen R., 2011, MNRAS, 411, 955
Mesinger A., McQuinn M., Spergel D. N., 2012, MNRAS, 422, 1403
Mesinger A., Ferrara A., Spiegel D. S., 2013, MNRAS, 431, 621
Mineo S., Gilfanov M., Sunyaev R., 2012, MNRAS, 419, 2095
Miralda-Escude J., 1998, ApJ, 501, 15
Miralda-Escudé J., 2003, ApJ, 597, 66
Miralda-Escudé J., Haehnelt M., Rees M. J., 2000, ApJ, 530, 1
Ono Y. et al., 2012, ApJ, 744, 83
Ouchi M. et al., 2010, ApJ, 723, 869
Pentericci L. et al., 2011, ApJ, 743, 132
Pentericci L. et al., 2014, ApJ, 793, 113
Planck Collaboration XVI, 2013, preprint (arXiv:1303.5076)
Rahmati A., Pawlik A. H., Raičević M., Schaye J., 2013, MNRAS, 430, 2427
Santos M. R., Ellis R. S., Kneib J.-P., Richard J., Kuijken K., 2004, ApJ, 606, 683
Schaye J., 2001, ApJ, 559, 507
Schenker M. A., Ellis R. S., Konidaris N. P., Stark D. P., 2014, ApJ, 795, 20
Shapiro P. R., Giroux M. L., 1987, ApJ, 321, L107
Shapiro P. R., Giroux M. L., Babul A., 1994, ApJ, 427, 25
Shibuya T. et al., 2014, ApJ, 788, 74
Sobacchi E., Mesinger A., 2013, MNRAS, 432, L51
Sobacchi E., Mesinger A., 2014, MNRAS, 440, 1662
Spitzer L., 1978, Physical Processes in the Interstellar Medium. Wiley, New York
Stark D. P., Ellis R. S., Chiu K., Ouchi M., Bunker A., 2010, MNRAS, 408, 1628
Steidel C. C., Erb D. K., Shapley A. E., Pettini M., Reddy N., Bogosavljević M., Rudie G. C., Rakic O., 2010, ApJ, 717, 289
Taylor J., Lidz A., 2014, MNRAS, 437, 2542
The Enzo Collaboration, 2014, ApJS, 211, 19
Tilvi V. et al., 2014, ApJ, 794, 5T
Treu T., Trenti M., Stiavelli M., Auger M. W., Bradley L. D., 2012, ApJ, 747, 27
Treu T., Schmidt K. B., Trenti M., Bradley L. D., Stiavelli M., 2013, ApJ, 775, L29
Verhamme A., Schaerer D., Atek H., Tapken C., 2008, A&A, 491, 89
Wyithe S., Bolton J. S., 2011, MNRAS, 412, 1926
Zahn O., Mesinger A., McQuinn M., Trac H., Cen R., Hernquist L. E., 2011, MNRAS, 414, 727

This paper has been typeset from a TEX/LATEX file prepared by the author.

Downloaded from https://academic.oup.com/mnras/article-abstract/446/1/566/1322451 by guest on 03 June 2020